Materials Advances

ROYAL SOCIETY OF CHEMISTRY

PAPER

View Article Online
View Journal | View Issue

Cite this: *Mater. Adv.*, 2025, **6**, 1889

Development of low-shrinkage eco-friendly composite materials for the DLP 3D printing technique

Wei-Chun Lin, *[a] Jui-Fu Tang,[a] Chia-Cheng Cheng,[a] Chia-Chien Kuo[a] and Wei-Hsuan Hung[b]

Received 17th July 2024,
Accepted 4th February 2025

DOI: 10.1039/d4ma00722k

rsc.li/materials-advances

3D printing technology has emerged as a production method in the past ten years and has attracted great attention in the market. Among various printing systems, digital light processing (DLP) 3D printing has extremely high planar resolution with a smooth sample surface, which is the best advantage of this technology. However, this 3D printing technology currently has three major challenges that urgently need to be improved: (1) the sample has dimensional shrinkage defects after secondary light curing; (2) the mechanical properties of the printed product have a serious tendency to decrease after secondary curing; and (3) the choice of printing materials used lacks diversification. The aforementioned defects will seriously affect the yield of printed products in high-precision manufacturing. In this research, eco-friendly carbon black has been added to the photosensitive resin of DLP to form composites. The mechanical properties of the material, thermogravimetric analysis, material viscosity, surface morphology and size shrinkage were investigated. In the tensile test, the area after the yield point is also significantly prolonged, which indicates better toughness of the composite resins. Adding recycled carbon black to the material can also enhance the heat resistance and thermal stability of the resin without increasing the solution viscosity. The newly synthesized composite resin demonstrated an improved hardness without severe size shrinkage after the post UV curing process, and also provided a new solution to the issue of abandoned tires.

1. Introduction

Additive manufacturing (AM) technologies, which build 3 dimensional (3D) structures layer-by-layer, provide a cost-effective alternative to create diverse objects in a short time.[1] Due to the advantages of 3D printing technology, that is a short processing time and low cost, there have been increasing discussions on 3D printing technology regarding the printing cycle, resolution, and materials in the past decades.[2] Whether for individuals or companies, 3D printing technology provides a convenient way to realize complex personalized products that are difficult to fabricate using traditional manufacturing methods.[3] With the advancement of 3D printing technology, it has gradually changed from industrial production to popularization in civil use.[4,5] In addition, the polymers used in 3D printing have long evolved from expensive monolithic materials to easy-to-produce components along with the rapid development of materials science and are not limited to a single aspect (Fig. 1).

Among several AM processes, there are three primary printing technologies. Fused filament fabrication (FFF) technology can easily print large-scale objects, but the printing resolution of FFF is the lowest among 3D printing due to the restriction of the tip size.[14] Selective laser sintering (SLS) technology allows the printing of diverse materials with better resolution, such as metals and metallic oxides.[15] However, the long printing cycle and expensive instruments of the SLS machine cause difficulties in popularization among civilians.[16,17] Vat photopolymerization, which includes stereolithography (SLA) and digital light processing technology (DLP), is a popular printing technique due to its excellent resolution. Compared to the FFF system, it provides higher resolution and a stronger structure to the 3D model. The main difference between SLA and DLP is the approach used to cure the layers. With SLA, a laser is utilized, whereas with DLP, a projector is employed.[18] In addition, LCD (liquid crystal display) technology, which is one of the DLP technologies and approaches used to cure the layers *via* liquid crystal displays, is used in this article.[19] Due to these advantages, DLP 3D printing has undergone rapid development in recent years and has been widely used in

[a] *Department of Photonics, National Sun Yat-sen University, Kaohsiung, Taiwan, Republic of China. E-mail: wclin@mail.nsysu.edu.tw*
[b] *Institute of Materials Science and Engineering, National Central University, Taoyuan, Taiwan, Republic of China*

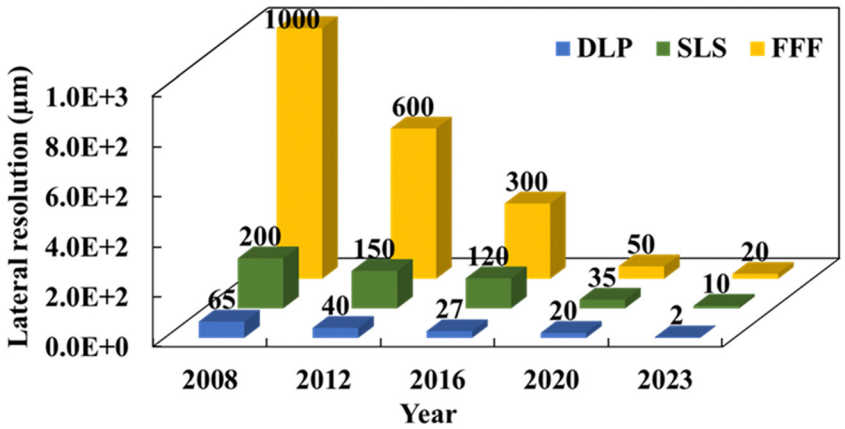

Fig. 1 The resolution of the common 3D printing technique in recent decades.[6–13]

dentistry technology,[20] jewelry manufacturing,[21,22] medicine,[23] biological metamaterials,[24] and shape-shifting structures.[25] However, there are some major drawbacks in the DLP technique that need to be improved before proceeding to wider applications. The first issue is the limited selection of DLP printing materials.[26] DLP printing materials lack a variety of mechanical properties, which limits the range of subsequent processing.[27] In addition, the post-curing process is necessary to ensure complete curing of the resin in SLA/DLP printed 3D models and preserve their geometric integrity. Higher mechanical properties are also obtained due to the solidification of excessive resin on the surface. However, the issue of shrinkage during post-curing needs to be addressed.[28] The commercial 3D printed resins commonly used, such as Phrozen ABS-like which was used in this study, are similar to other commercial 3D printed resins in terms of shrinkage (approximal 0.4%) in length, width, and height directions during secondary (post) UV curing;[29] the DLP 3D printing and post curing process is shown in Fig. 2b and c. This shrinkage issue has a huge impact on the industries that need to control sample dimensions precisely. One of the best solutions to solve these two issues is to develop a photosensitized resin with various properties. Therefore, we turned our attention to synthesize composite resins.

Tires are a highly engineered and complex assemblage of components that possess a wide range of properties.[30,31] Today's tires have a very complicated engineering structure that has evolved from a simple wheel into a modern pneumatic tire.[30,32] The major component used to construct a tire comprises rubber, and other components include carbon black, metals, textiles, and a variety of additives.[33] Tires constructed from these dissimilar materials form a highly complex structure, so that tires

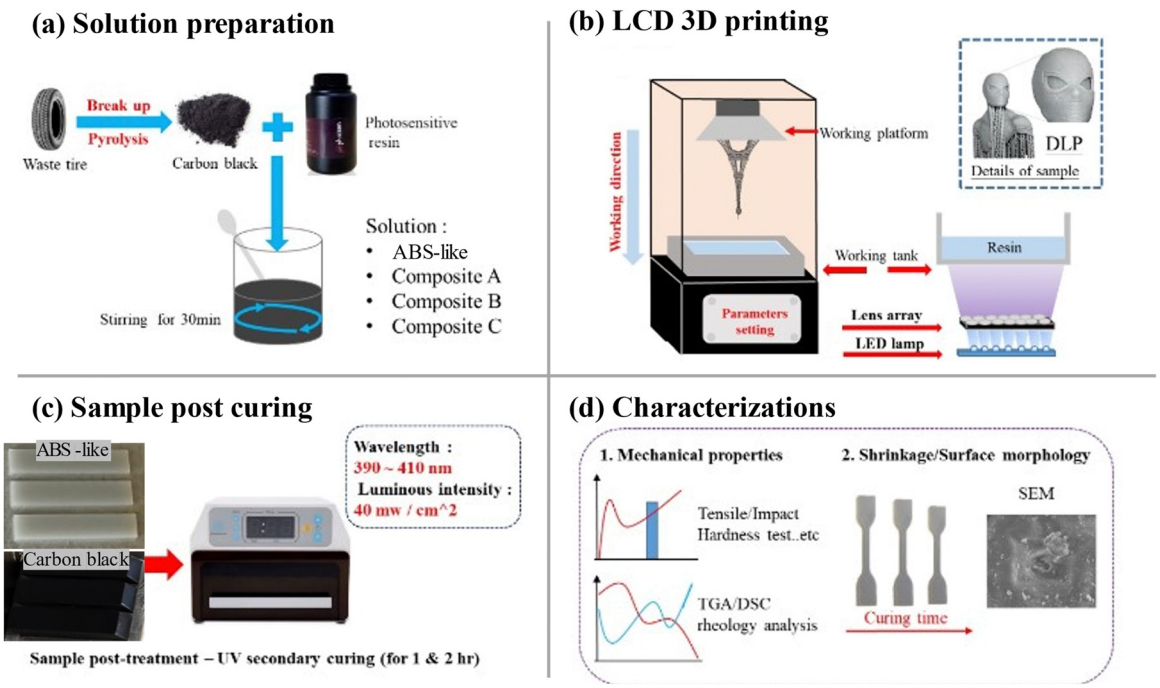

Fig. 2 Schematic of the process of 3D printed specimens with eco-friendly CB as additives. (a) Photopolymer preparation. (b) DLP 3D printing process and the delicate features. (c) Sample posttreatment for 1 and 2 hours. (d) Materials characterizations.

can operate in a wide range of environments.[34] In the past, waste tires became a serious problem that was difficult to handle in terms of recycling due to their bulky volume and inconvenience.[35] In tropical and subtropical regions, excessive waste tires accumulated and formed puddles after rain, leading to dengue fever and other problems induced by the mosquito. In previous decades, several methods for recycling and reusing tires appeared. Whole waste tires are usually reused as buffering layers in playground equipment, highway crash barriers, breakwaters, and floatation devices. Some waste tires are shredded into crumbs and used as an additive of composite materials in polymeric industries to form products such as mats or special playground surfaces.[36] Moreover, researchers have developed decomposition methods to chemically convert waste tires into high-performance carbon materials, which endows them with new use value.[37] For example, pyrolysis is the process of decomposing the rubber component of shredded tires in the presence of heat and the absence of oxidation.[38] The yield of pyrolysis contains the basic chemicals used to make a tire, such as carbon black, sulfide, zinc, oils, and gas.

In this study, pyrolyzed carbon black (CB) from shredded tires was surface-functionalized as different kinds of CB, as shown in Fig. 2a. The diversity of their mechanical properties is achieved by blending different functionalized CBs with photosensitized ABS-like resin purchased from Phrozen Tech. Co, Ltd, Taiwan. The well-dispersed composite photopolymer resin is cured under a panel of light sources (405 nm), which is coordinated by a lens array, as shown in Fig. 2b. The samples underwent post-treatment for 1 hour to ensure complete curing and for 2 hours to observe significant resin shrinkage[39] (Fig. 2c). A series of material analysis was used to investigate the mechanical properties, thermal stability, rheology, shrinkage and morphology of the composite photopolymer resins (Fig. 2d). In this study, the shrinkage issue was significantly reduced, and more ductile material was achieved after 1 hour post-treatment by the newly synthesized CB-assisted composite resin.

2. Materials and methods

2.1. The preparation for printing resin composites A, B and C

The carbon black (CB) used in this research originated from the recycling of waste tires obtained from Enrestec Tech (Taiwan) with a series of crushing and pyrolysis processes. A vacuum pump is used to quickly extract the gas from the reactor. The product is first converted to heavy oil or light oil through the oil–gas condensing purge tank and the deaerator, while the gas that has not been condensed can be sent to the combustion tower. The heat generated by combustion can be used to provide dry recovery of carbon black or the required thermal energy of waste tire pyrolysis. To blend with polymeric resin, the carbon black must be shredded into particles using magnetic separation, including the ball milling and the drying process. Submicron-scale CB (50–200 nm) was then further synthesized with different surface functionalized groups, such as sulfurized CB, desulfurized CB and polyurethane-encapsulated CB. The photosensitizing resin was purchased from Phrozen Tech. Co, Ltd, Taiwan. An opaque tank was used to pour 299.7 g of photosensitive resin, and 0.3 g of sulfurized, desulfurized, and polyurethane-encapsulated carbon black were each added to configure a composite resin solution containing 0.1 wt%. For easier description, the composite resins with sulfurized CB, desulfurized CB and polyurethane-encapsulated CB as additives were named after composites A, B and C, respectively.

2.1.1. Sulfurized CB (composite A). First, 2 g CB and 300 mL CH_2Cl_2 were mixed in a 500 mL three-neck round-bottom flask with an ultrasonic cleaner at a frequency of 40 Hz for 30 min. Then, 0.3 M $KMnO_4$ and 1.55 M tetrabutyl ammonium bromide (TBABr) were dissolved in deionized water mixed with 80 mL acetic acid and stirred (300 rpm) at ambient temperature for 24 hours. After that, the solid product was separated from the mixture solution by centrifugation and filtration and washed sufficiently with methanol and deionized water. This purification process was repeated at least five times. Finally, the separated product was dried in a vacuum oven at 100 °C for 24 hours.

2.1.2. Desulfurized CB (composite B). Different volumes of H_2O_2 and formic acid (1 : 1 by volume) were added to 100 mL of crude oil. The ultrasonic probe was immersed in the center of the beaker at approximately 3/4 of the depth of the oil sample, and the action mode and intermittent time of 2 s action time were selected. Subsequently, the oil sample was subjected to magnetic stirring for 1 h after ultrasonic cleaning. A single-factor experiment was conducted to use the control variable method. The ultrasonic cleaner power was controlled to 80 W, the irradiation time was set to 10 min, and the amount of oxidant was 10 mL. A mixture of 20 mL of acetonitrile, 20 mL of methanol, and 20 mL of water was added for extraction. The extracted mixture was slowly transferred into a separator funnel and allowed to sit for 10 min until the extracted mixture no longer increased.[40]

2.1.3. Polyurethane-encapsulated CB (composite C). Polyurethane-encapsulated CB is one of the derivatives based on sulfurized CB (composite A). Three grams of primary-like sized carbon black (PCB) nanoparticles and 300 mL of CH_2Cl_2 were put into a baffled double-layered flask, and the mixture was dispersed using ultrasonication (80 W, Digital PRO$^+$, PHROZEN Tech. Co., Ltd) for 2 hours in the flask. After this, aq. 50 wt% TBABr with a concentration of 1.86 M was dissolved in 50 mL of deionized (DI) water. The diluted solution, 120 mL of acetic acid, and 0.47 M $KMnO_4$ dissolved in 50 mL of DI water were added to the flask and stirred vigorously for 24 h. The CB nanoparticle-based mixture was then washed, settled using centrifugation, and redispersed in MeOH/DI water (volume ratio of 8 : 2). The MeOH/DI water washing process was repeated a minimum of five times. After vacuum freeze-drying, hydroxyl group-modified PCB (CB-OH) nanoparticles were obtained.[41]

2.2. The 3D printing process and sample posttreatment

The A.STL 3D model file of tensile and impact test specimens was found elsewhere.[42] CHITU BOX (3D slicing software) is used to modify the 3D printing file. The thickness of every slice layer is 0.05 mm. The impact test specimen slices 200 layers, and the tensile test specimen slices 40 layers. The curing time of every layer is 8 seconds. After completing the modification,

the file will be uploaded into the 3D printer. The LCD 3D printer is Phrozen Shuffle 2018 2K supplied by Phrozen Tech. The composite resin solution was placed into the ultrasonic cleaner and shaken for 30 minutes to evenly disperse the carbon black. Then, the composite resin solution to be printed was poured, and the poured resin only needed the 2/3 capacity of the slot mold. An excessive amount of resin will cause the solution to overflow the slot mold during printing and then penetrate the 3D printer and damage the LCD panel. The standard deviation in figures is based on 9 samples of each recipe. Before post-curing, the architecture of the 3D-printed samples is created using a patterned digital light processing technique. The composite resin contains only 0.1 wt% CB additives, ensuring that the viscosity—a critical factor for successful 3D printing—remains largely unaffected. To assess the effect of the filler during post-curing, we simplified the 3D printer settings, resulting in a uniform slice thickness for each layer of the samples. Generally, a post-curing duration of approximately 1 hour is necessary to enhance mechanical properties and solidify any residual resin on the sample surface. The 2-hour post-curing duration was then chosen to observe the shrinkage effect more clearly. After printing was complete, the printed sample was cleaned with alcohol several times and then placed in a post-curing lamp for secondary curing. The post-curing lamp is purchased from Phrozen Tech. The wavelength emitted by the UV lamp was 390–410 nm, and the light intensity was 40 mW cm^{-2}. After secondary curing, physical properties such as tensile, impact, shrinkage, hardness, and surface morphology were measured.

2.3. Material characterizations

2.3.1. Mechanical characterization. The mechanical properties were measured by a computer-based universal material testing machine purchased from Chun Yen Testing Machines Co., Ltd, Taiwan. The 3D printed specimen was measured through a universal testing machine to explore the material properties of the composite printing resin. The specimen for the tensile test was 75 mm long, 12 mm wide and 2 mm thick. The specimen's printing direction was vertically aligned along the height axis. The punctuation range for the tensile test was 20 cm with a tension velocity of 50 mm min^{-1}. The impact testing for the specimen was 55 mm in length, 10 mm in width and 10 mm in thickness with a 100 mm^2 sample testing area. The elevation degree of the pendulum hammer was 90° with a weight of 30 kg. The specimen hardness was tested by a shore-D durometer, which is specified for the hardness analysis of rubber and plastics.

2.3.2. Thermogravimetric analysis (TGA). Samples were heated from 25 °C to 600 °C at a ramp rate of 5 °C min^{-1} in aluminum pans using a TA-TGA (TA instruments, TGA-2950, Waters, LLC, USA). Nitrogen was used as a purge gas with a flow rate of 25 mL min^{-1}. Data collection and analysis were performed by TA Instruments Trios software, and the weight lost/onset temperature was calculated.

2.3.3. Differential scanning calorimetry (DSC). Measurements were performed by MDSC 2920 (TA Instruments, Waters, LLC, USA) with a heating rate of 5 °C min^{-1} in a nitrogen atmosphere. The weight of each sample was approximately 1.6 mg. It was first quickly heated from 25 to 100 °C, and then the sample was cooled to 25 °C at a cooling rate of 5 °C min^{-1}.

2.3.4. Viscosity. An Anton Paar (Graz, Austria) MCR 302 rheometer with an H-ETD 400 electrical temperature device was used for temperature-dependent viscosity measurement between 30 °C and 105 °C. The analysis was performed with a 5 s^{-1} shear rate at a heating rate of 3.6 °C min^{-1}.

2.3.5. Shrinkage measurement. The shrinkage of the samples was assessed by anisotropic retraction[43] (length, width, thickness). The sample sizes were measured before and after the UV posttreatment step for 1 and 2 hours using a digital micrometer. The post-curing process is conducted within a machine equipped with a 405 nm UV light source. The carrier platform inside has the capability to rotate 360°, ensuring uniform post-curing of the specimens. The shrinkage of the sample was calculated with the following formula: S (%) = $[1 - (d_{\text{after UV curing}}/d_{\text{before UV curing}})] \times 100\%$. The standard deviation is based on 9 sample measurements of each composite resin material. For each measurement, an averaged value was calculated based on three repeated measurements.

2.3.6. Scanning electron microscope (SEM). SEM images were obtained with an FEI Nova200 Nano scanning electron microscope operated at 5 kV. The surface morphology of the printed specimen was examined under low vacuum mode. The imaging area is the cross-sectional region of the specimen after the tensile test. The specimen was dried by nitrogen flow before applying a thin Au coating layer for better conductivity.

3. Results and discussion

3.1. Mechanical properties

The material properties of the ABS-like resin with different functionalized CB as additives are illustrated in Fig. 3 and listed in Table 1. As shown in Fig. 3a, the ABS-like exhibits a sharp yield point. On the other hand, the stress–strain curve for composite B does not exhibit a sharp yield point. Composites A and C show a wide range of extended areas between the upper and lower yield points, which corresponds to an appreciable plastic strain at an almost constant stress. In the sample cured for one and two hours (red curves between Fig. 3a and b) after the yield point, indicating that a higher strain rate can be obtained with lower stress, this plateau area is more conducive for processing with diverse industrial applications. While ABS-like resin containing 0.1 wt% desulfurized CB (composite B) has no obvious yield point after curing for two hours (Fig. 3b), indicating that the addition of carbon black containing sulfur is important.

The composite A resin performs the best in terms of impact resistance after curing for one and two hours, which could be attributed to the addition of 0.1% sulfurized carbon black (Fig. 3c). The range of the standard deviation is reduced, indicating that the impact resistance and stability of the composite A resin are stronger. The resin can be applied in orthopedics, dental molds, and other materials that require high strength. Otherwise, the worst impact value and standard deviation are

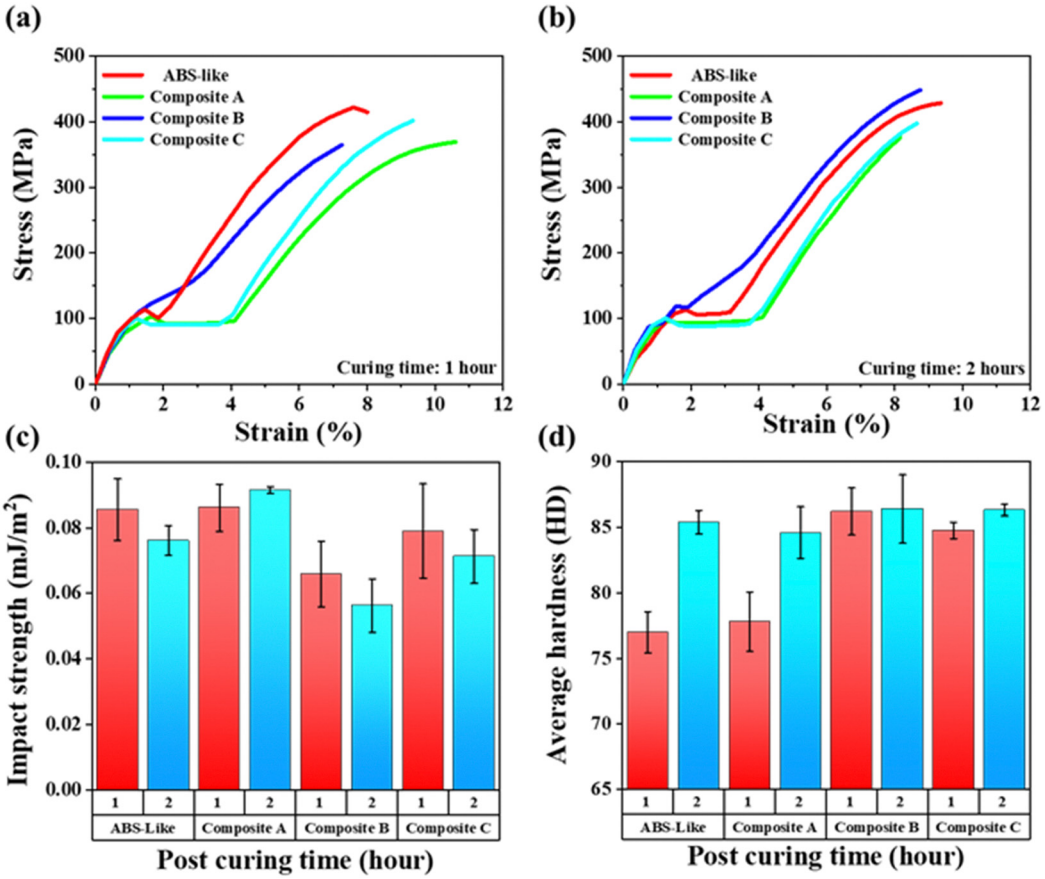

Fig. 3 Mechanical properties test. (a) Tensile test with 1 hour of UV curing, (b) tensile test with 2 hours of UV curing, (c) impact test with UV curing for 1 and 2 hours, and (d) hardness test with UV curing for 1 and 2 hours of ABS-like and composites A, B and C.

obtained by composite B and composite C. In summary, carbon black decorated with sulfur (composite A) could achieve a better impact value and material stability. In terms of hardness (Fig. 3d), all resins show an increase in hardness after 2 hours post-curing. Composite A shows similar mechanical properties to the ABS-like resin. Both show a significant increase in hardness after 2 hours of curing (Fig. 3d). Composite B and Composite C achieve hardness comparable to that of the resin cured for 2 hours with only 1 hour of post-curing. In this way, the post-curing time can be reduced to achieve a similar hardness value to that after 2 hours curing. The reduced curing time could also benefit reduced shrinkage due to post-curing. The detailed data of each specimen after the tensile, impact and hardness tests are shown in Table 1.

3.2. Thermal and rheology analysis of materials

The thermal analysis of the composite resins is shown in Fig. 4a. The glass transition temperature of ABS-like resin is ~70 °C. From the TGA and DSC analysis, it is indicated that the ABS-like resin without adding carbon black is easily degraded

Table 1 The mechanical properties of ABS-like resin with 0.1 wt% added composite material

Curing time	ABS-like[a]	Composite A (ABS + sulfurized CB)	Composite B (ABS + desulfurized CB)	Composite C (ABS + functional CB)
Tensile test (stress–strain)[b]				
UV 1 hour	414.6/8.15%	369.2/10.60%	364.6/7.25%	401.5/9.35%
UV 2 hour	428.3/9.35%	375.8/8.15%	448.2/8.75%	397.5/8.65%
Impact strength (mJ m^{-2})				
UV 1 hour	0.0855 ± 0.0093	0.0861 ± 0.00771	0.0659 ± 0.0100	0.0790 ± 0.0143
UV 2 hour	0.0761 ± 0.0045	0.0914 ± 0.0010	0.0563 ± 0.0082	0.0713 ± 0.0082
Hardness (unit)				
UV 1 hour	77.0 ± 1.6	77.8 ± 2.3	86.2 ± 1.8	848 ± 0.6
UV 2 hour	85.4 ± 0.9	84.6 ± 2.0	86.4 ± 2.6	86.3 ± 0.4

[a] The regional ABS-like resin purchased from Phrozen Co. Ltd with the recipe consisting of photo-initiator, reactive diluent, crosslinker and acrylonitrile–butadiene–styrene. [b] The average value based on 15 specimen tests at the fracture point.

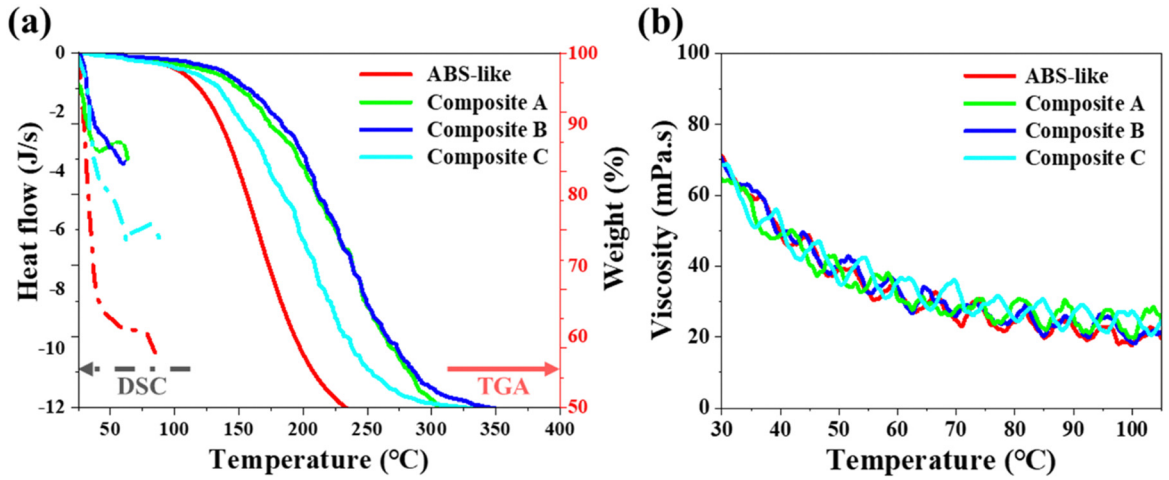

Fig. 4 (a) Thermal analysis of ABS-like resin and composites A, B and C with TGA (solid line) and DSC (dashed line). (b) Rheology test on ABS-like and composites A, B and C.

compared to other composites. It can be observed that the ABS-like resin sample has the largest exothermic rate. From the thermal analysis of different composite resins, it is concluded that the addition of carbon black with different additives in ABS-like resin can effectively improve the thermal stability of materials. The rheological behavior of all resins is shown in

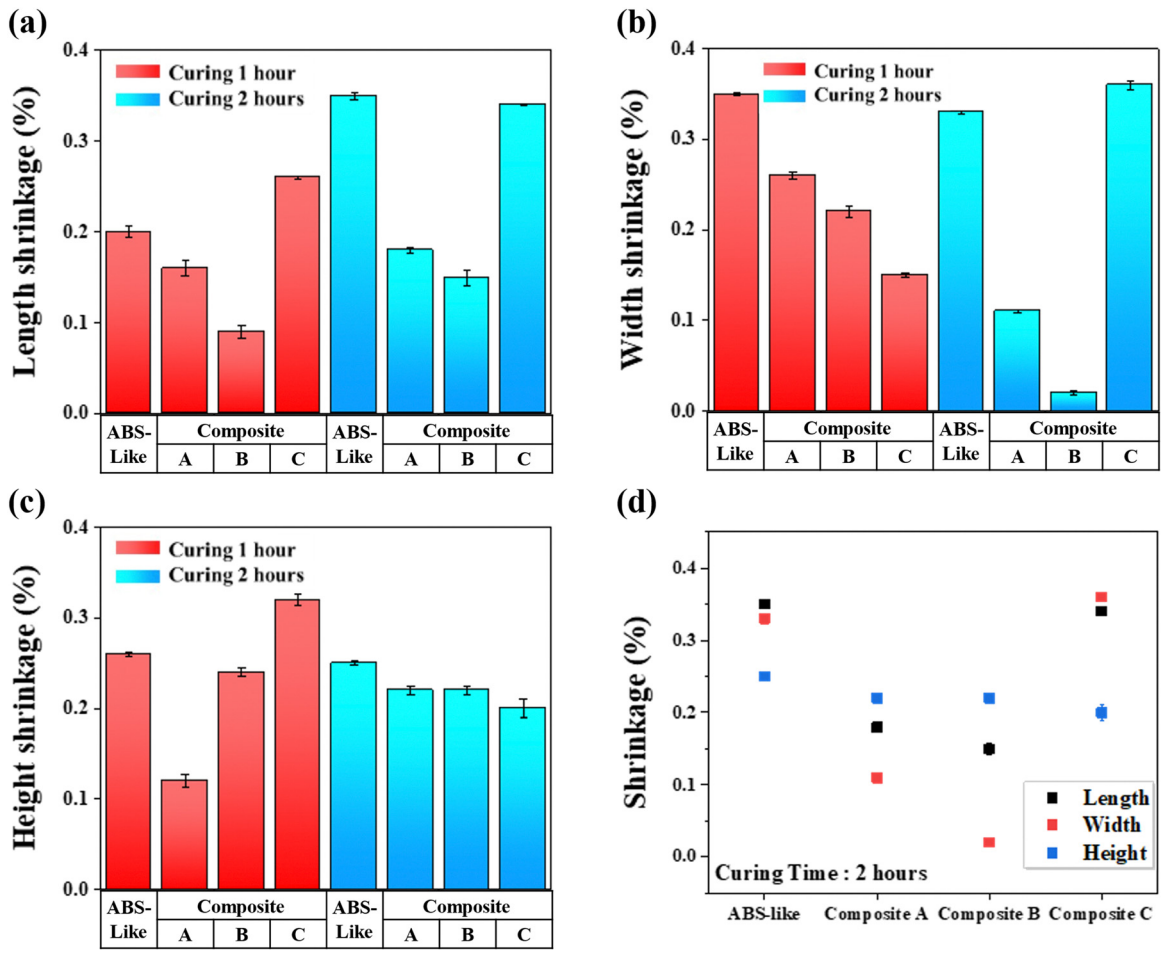

Fig. 5 The shrinkage of ABS-like resin and composites A, B and C on the (a) length, (b) width, (c) height side after 1 and 2 hours of curing and (d) the shrinkage comparison in length, width, and height of composite materials. The standard deviation is based on the measurements of nine specimens.

Table 2 The shrinkage of ABS-like and composites A, B and C after UV curing for 1 and 2 hours

Curing time	ABS-like[a]	Composite A (ABS + sulfurized CB)	Composite B (ABS + desulfurized CB)	Composite C (ABS + functional CB)
Length (%)				
UV 1 hour	0.202 ± 0.006	0.168 ± 0.008	0.099 ± 0.007	0.261 ± 0.001
UV 2 hour	0.349 ± 0.004	0.182 ± 0.003	0.158 ± 0.008	0.349 ± 0.001
Width (%)				
UV 1 hour	0.352 ± 0.002	0.260 ± 0.004	0.220 ± 0.006	0.149 ± 0.002
UV 2 hour	0.333 ± 0.001	0.112 ± 0.001	0.023 ± 0.0003	0.360 ± 0.005
Height (%)				
UV 1 hour	0.265 ± 0.002	0.119 ± 0.007	0.241 ± 0.005	0.320 ± 0.007
UV 2 hour	0.253 ± 0.002	0.220 ± 0.005	0.226 ± 0.004	0.200 ± 0.010

[a] The regional ABS-Like resin purchased from Phrozen Co. Ltd. with the recipe consisting of photo-initiator, reactive diluent, crosslinker and acrylonitrile–butadiene–styrene.

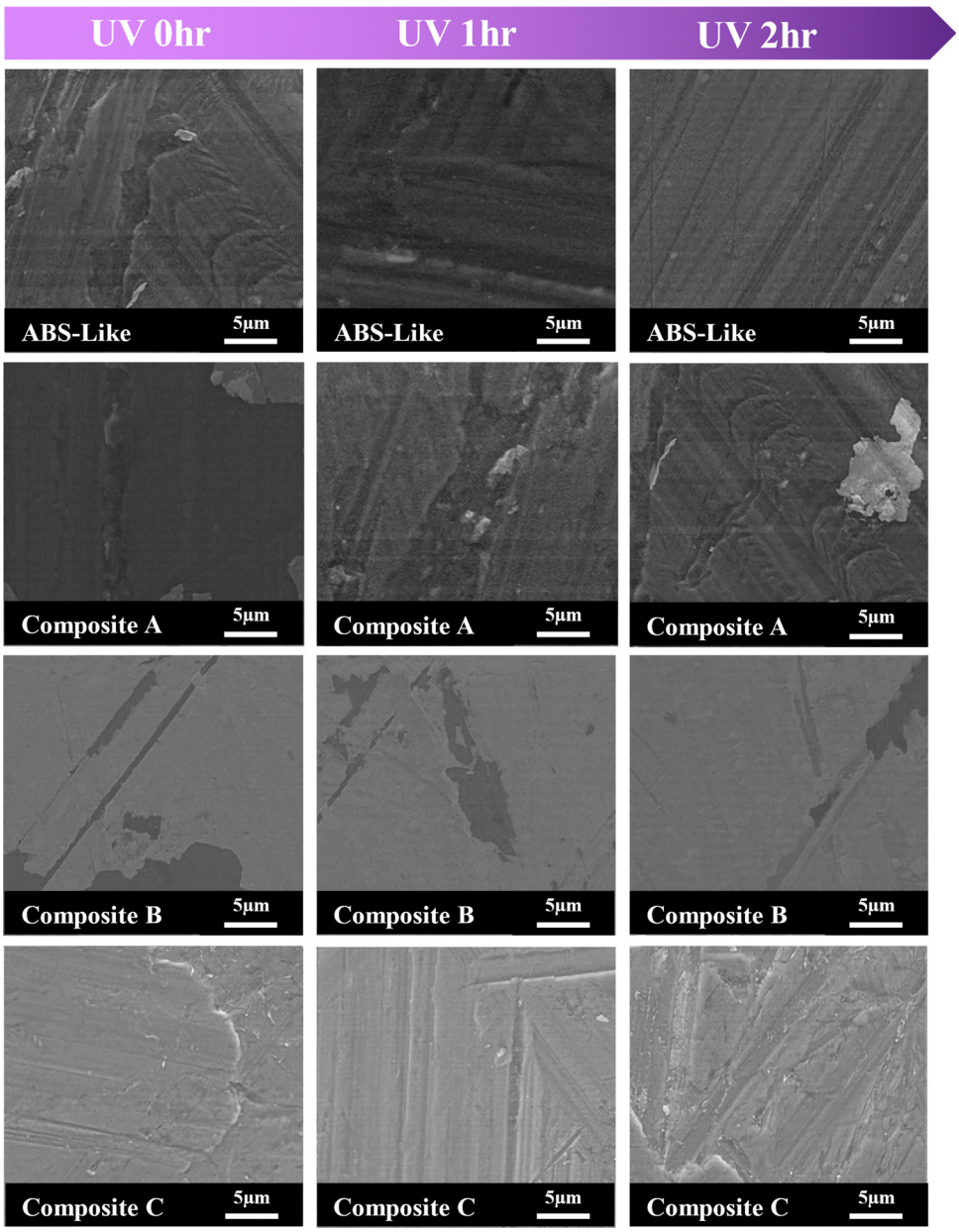

Fig. 6 The surface morphology of the horizontal section of the ABS-like resin, composite A sample, composite B sample and composite C sample.

Fig. 4b. The viscosity of the sample showed consistency after adding carbon black, indicating that not only did the composite materials not change the viscosity when heated to 105 °C but also increased the thermal stability. This result shows that adding carbon black could enhance mechanical properties without obvious changes in the viscosity.

3.3. Shrinkage measurements

The shrinkage test with different composite materials is shown in Fig. 5 and Table 2. To observe the shrinkage effect more clearly, 2-hour post-curing was used to prolong the UV exposure duration. Comparing the sample shrinkage in ABS-like and composite A and B, it is proved that composite A and B significantly improve the shrinkage after UV curing for 1 and 2 h. In Fig. 5a and b, composite B demonstrated the best performance with the lowest shrinkage ratio, which is due to the less flexibility of the desulfurized carbon black. Nevertheless, significant differences in length and width shrinkage are observed between 1 hour and 2 hours of post-curing, suggesting that the carbon black particles may not be evenly distributed within the composite resin. Except for composite C, the carbon black additive acts as an obstacle during crosslinking and the post-curing process. Therefore, composite A and B exhibit better anti-shrinkage performance. In contrast, composite C decorated with polyurethane-encapsulated does not show better anti-shrinkage performance than other composites, which indicates that the carbon black modified with this polymeric material offers large flexibility to resin. The larger flexibility of composite C totally reflects the characteristic of the polyurethane, which is well-known for its applications in flexible foams. Therefore, the large molecular weight of polyurethane provides a good strain effect during UV exposure. This shrinkage result is consistent with the tensile test as shown in Fig. 3 and Table 1. The comparison of the shrinkage ratio between ABS-like resin, composite A and B is shown in Fig. 5d.

3.4. Surface morphology of the cross section after a tensile test

Fig. 6 shows the surface morphology of all resins with different UV exposure durations. It could be observed that the carbon black grains disperse uniformly in the ABS-like resin. It is noted that the cross-section areas of composite B are flat. Compared to other resins with several deep fracture lines at the cross-section areas after tensile testing, composite B proved that the desulfurized CB additive makes the resin more brittle at the fracture point. The flat cross section of composite B during the tensile test is a reverse proof of the excellent shrinkage performance obtained in Fig. 5. Furthermore, the larger size of the additive and irregular facture lines in composite C images proved that polyurethane-encapsulated CB may provide better strain, which lead to a higher shrinkage ratio. The morphology has no obvious difference between samples with different treatment times.

4. Conclusions

The dimensional shrinkage issue, one of the most crucial problems in DLP 3D printing technology, has been solved by incorporating eco-friendly carbon black as additives. The results demonstrated that adding carbon black can improve the toughness of the specimen, and the extent area after the yield point also rises significantly, which is beneficial to processing applications. With the tensile test, it was observed that adding 0.1 wt% sulfurized carbon black into the ABS-like resin shows the best impact resistance. The composite B (desulfurized carbon black) and composite C (polyurethane-encapsulated) demonstrated a significant improvement in hardness. The thermal and rheological analysis indicated that the addition of carbon black not only improved the thermal stability, but also retained the viscosity of the composite resin. The shrinkage issue could be alleviated with the sulfurized and desulfurized carbon black as additives, which is due to the compact structure with carbon black particles as obstacles. This obstacle plays a role to stop resin shrinkage upon exposure to UV light. Therefore, the new synthesized eco-friendly composites not only provide a diverse mechanical property of the resin, but also solve the shrinkage issue during the post-curing process, which is a significantly breakthrough for the additive manufacturing technology. In addition, using carbon black as an additive in photo-sensitive resin offers a new way to solve the urgent environmental issue caused by waste tires.

Data availability

All data generated or analyzed during this study are included in this published article. The raw data is available upon request. There is no crystal structure data presented in this article. Data for this article, including the resolution of the common 3D printing technique are available in ref. 6–13 and 29.

Conflicts of interest

There are no conflicts to declare.

Acknowledgements

The authors acknowledge sponsorship by the National Science and Technology Council (NSTC, Taiwan) through grant number MOST 110-2622-E-110-017, NSTC 111-2622-E-110-019 and NSTC 113-2622-E-110-005. This work was financially supported by the ''High Entropy Materials Center'' from The Featured Areas Research Center Program within the framework of the Higher Education Sprout Project by the Ministry of Education (MOE) and from the Project MOST 110-2221-E-008-045-MY3, NSTC 112-2221-E-A49-027- and NSTC 113-2221-E-A49-003- by National Science and Technology Council (NSTC) in Taiwan. The authors acknowledge technical and instrument support from Phrozen Tech. Co. Ltd, Taiwan. The authors acknowledge material support from Enrestec Co. Ltd, Taiwan.

References

1 T. D. Ngo, A. Kashani, G. Imbalzano, K. T. Q. Nguyen and D. Hui, Additive manufacturing (3D printing): A review of

materials, methods, applications and challenges, *Composites, Part B*, 2018, **143**, 172–196, DOI: 10.1016/J.COMPOSITESB.2018.02.012.

2 J. Y. Lee, J. An and C. K. Chua, Fundamentals and applications of 3D printing for novel materials, *Appl. Mater. Today*, 2017, **7**, 120–133, DOI: 10.1016/J.APMT.2017.02.004.

3 S. El-Sayegh, L. Romdhane and S. Manjikian, A critical review of 3D printing in construction: benefits, challenges, and risks, *Archives Civil Mech. Eng.*, 2020, **20**, 1–25, DOI: 10.1007/s43452-020-00038-w.

4 M. Kalender, S. E. Kilic, S. Ersoy, Y. Bozkurt and S. Salman, Additive manufacturing and 3D printer technology in aerospace industry, Proceedings of 9th International Conference on Recent Advances in Space Technologies, RAST 2019, 2019, pp. 689–695, DOI: 10.1109/RAST.2019.8767881.

5 A. Jandyal, I. Chaturvedi, I. Wazir, A. Raina and M. I. Ul Haq, 3D printing – A review of processes, materials and applications in industry 4.0, *Sustainable Operat. Comput.*, 2022, **3**, 33–42, DOI: 10.1016/J.SUSOC.2021.09.004.

6 S. Barone, P. Neri, A. Paoli, A. V. Razionale and F. Tamburrino, Development of a DLP 3D printer for orthodontic applications, *Procedia Manuf.*, 2019, **38**, 1017–1025, DOI: 10.1016/J.PROMFG.2020.01.187.

7 S. C. Ligon, R. Liska, J. Stampfl, M. Gurr and R. Mülhaupt, Polymers for 3D Printing and Customized Additive Manufacturing, *Chem. Rev.*, 2017, **117**, 10212–10290, DOI: 10.1021/acs.chemrev.7b00074.

8 S. Barone, P. Neri, A. Paoli and A. V. Razionale, Design and manufacturing of patient-specific orthodontic appliances by computer-aided engineering techniques, *J. Eng. Med.*, 2017, **232**, 54–66, DOI: 10.1177/0954411917742945.

9 Y. Han, C. Wei and J. Dong, Super-resolution electrohydrodynamic (EHD) 3D printing of micro-structures using phase-change inks, *Manuf. Lett.*, 2014, **2**, 96–99, DOI: 10.1016/J.MFGLET.2014.07.005.

10 M. Launhardt, A. Wörz, A. Loderer, T. Laumer, D. Drummer, T. Hausotte and M. Schmidt, Detecting surface roughness on SLS parts with various measuring techniques, *Polym. Test.*, 2016, **53**, 217–226, DOI: 10.1016/j.polymertesting.2016.05.022.

11 J. Valentinčič, M. Jerman, I. Sabotin and A. Lebar, Low Cost Printer for DLP Stereolithography Micromanufacturing View project IceJet View project, *J. Mech. Eng.*, 2017, **63**, 559–566, DOI: 10.5545/sv-jme.2017.4591.

12 A. Amini, R. M. Guijt, T. Themelis, J. De Vos and S. Eeltink, Recent developments in digital light processing 3D-printing techniques for microfluidic analytical devices, *J. Chromatogr. A*, 1692, **2023**, 463842, DOI: 10.1016/J.CHROMA.2023.463842.

13 X. Wang, J. Liu, Y. Zhang, P. M. Kristiansen, A. Islam, M. Gilchrist and N. Zhang, Advances in precision microfabrication through digital light processing: system development, material and applications, *Virtual Phys. Prototyp.*, 2023, **18**, e2248101, DOI: 10.1080/17452759.2023.2248101.

14 R. B. Kristiawan, F. Imaduddin, D. Ariawan, Ubaidillah and Z. Arifin, A review on the fused deposition modeling (FDM) 3D printing: Filament processing, materials, and printing parameters, *Open Eng.*, 2021, **11**, 639–649, DOI: 10.1515/eng-2021-0063.

15 N. A. Charoo, S. F. Barakh Ali, E. M. Mohamed, M. A. Kuttolamadom, T. Ozkan, M. A. Khan and Z. Rahman, Selective laser sintering 3D printing – an overview of the technology and pharmaceutical applications, *Drug Dev. Ind. Pharm.*, 2020, **46**, 869–877, DOI: 10.1080/03639045.2020.1764027.

16 G. Hussain, W. A. Khan, H. A. Ashraf, H. Ahmad, H. Ahmed, A. Imran, I. Ahmad, K. Rehman and G. Abbas, Design and development of a lightweight SLS 3D printer with a controlled heating mechanism: Part A, *Int. J. Lightweight Mater. Manuf.*, 2019, **2**, 373–378, DOI: 10.1016/j.ijlmm.2019.01.005.

17 D. Pinheiro, K. R. Sunaja Devi, A. Jose, N. Rajiv Bharadwaj and K. J. Thomas, Effect of surface charge and other critical parameters on the adsorption of dyes on SLS coated ZnO nanoparticles and optimization using response surface methodology, *J. Environ. Chem. Eng.*, 2020, **8**, 103987, DOI: 10.1016/J.JECE.2020.103987.

18 A. Vlasa, V. I. Bocanet, M. H. Muntean, A. Bud, B. R. Dragomir, S. N. Rosu, L. Lazar and E. Bud, Accuracy of Three-Dimensional Printed Dental Models Based on Ethylene Di-Methacrylate-Stereolithography (SLA) vs. Digital Light Processing (DLP), *Appl. Sci.*, 2023, **13**, 2664, DOI: 10.3390/APP13042664.

19 H. Chen, D. H. Cheng, S. C. Huang and Y. M. Lin, Comparison of flexural properties and cytotoxicity of interim materials printed from mono-LCD and DLP 3D printers, *J. Prosthet. Dent.*, 2021, **126**, 703–708, DOI: 10.1016/J.PROSDENT.2020.09.003.

20 Y. Tian, C. X. Chen, X. Xu, J. Wang, X. Hou, K. Li, X. Lu, H. Y. Shi, E. S. Lee and H. B. Jiang, A Review of 3D Printing in Dentistry: Technologies, Affecting Factors, and Applications, *Scanning*, 2021, 9950131, DOI: 10.1155/2021/9950131.

21 Y. Kong, Application of 3D Printing Technology in Jewelry Design in the Era of Artificial Intelligence, *Adv. Intell. Syst. Comput.*, 2021, **1343**, 162–169, DOI: 10.1007/978-3-030-69999-4_22.

22 C. Chang, A Study on Jewelry Design Using 3D-Printing - Focusing on Curved Form, *J. Korea Convergence Soc.*, 2019, **10**, 189–194, DOI: 10.15207/JKCS.2019.10.4.189.

23 H. N. Chia and B. M. Wu, Recent advances in 3D printing of biomaterials, *J. Biol. Eng.*, 2015, **9**, 1–14, DOI: 10.1186/s13036-015-0001-4.

24 Y. Shen, H. Tang, X. Huang, R. Hang, X. Zhang, Y. Wang and X. Yao, DLP printing photocurable chitosan to build bioconstructs for tissue engineering, *Carbohydr. Polym.*, 2020, **235**, 115970, DOI: 10.1016/J.CARBPOL.2020.115970.

25 X. Wang, M. Jiang, Z. Zhou, J. Gou and D. Hui, 3D printing of polymer matrix composites: A review and prospective, *Composites, Part B*, 2017, **110**, 442–458, DOI: 10.1016/J.COMPOSITESB.2016.11.034.

26 D. W. Yee and J. R. Greer, Three-dimensional chemical reactors: in situ materials synthesis to advance vat photopolymerization, *Polym. Int.*, 2021, **70**, 964–976, DOI: 10.1002/PI.6165.

27 J. Borrello, P. Nasser, J. C. Iatridis and K. D. Costa, 3D printing a mechanically-tunable acrylate resin on a commercial DLP-SLA printer, *Addit Manuf.*, 2018, **23**, 374–380, DOI: 10.1016/J.ADDMA.2018.08.019.

28 M. Hegde, V. Meenakshisundaram, N. Chartrain, S. Sekhar, D. Tafti, C. B. Williams, T. E. Long, M. Hegde, T. E. Long, V. Meenakshisundaram, S. Sekhar, D. Tafti, C. B. Williams and N. Chartrain, 3D Printing All-Aromatic Polyimides using Mask-Projection Stereolithography: Processing the Nonprocessable, *Adv. Mater.*, 2017, **29**, 1701240, DOI: **10.1002/ADMA.201701240**.

29 Linear shrinkage of 3D-printing resins|Liqcreate, (n.d.). **https://www.liqcreate.com/supportarticles/linear-shrinkage-of-3d-printing-resins**/ (accessed March 6, 2024).

30 B. S. Thomas and R. C. Gupta, A comprehensive review on the applications of waste tire rubber in cement concrete, *Renewable Sustainable Energy Rev.*, 2016, **54**, 1323–1333, DOI: **10.1016/J.RSER.2015.10.092**.

31 M. A. Yazdi, J. Yang, L. Yihui and H. Su, A Review on Application of Waste Tire in Concrete, *Int. J. Civil Environ. Eng.*, 2016, **9**, 1656–1661, DOI: **10.5281/ZENODO.1338638**.

32 B. Adhikari, D. De and S. Maiti, Reclamation and recycling of waste rubber, *Prog. Polym. Sci.*, 2000, **25**, 909–948, DOI: **10.1016/S0079-6700(00)00020-4**.

33 H. Z. Chu, D. Liu, Z. W. Cui, K. Wang, G. X. Qiu and G. Y. Liu, Effect of crosslink density on solubility parameters of styrene butadiene rubber and the application in pre-screening of new potential additives, *Polym. Test.*, 2020, **81**, 106253, DOI: **10.1016/j.polymertesting.2019.106253**.

34 K. Stevenson, B. Stallwood and A. G. Hart, Tire Rubber Recycling and Bioremediation: A Review, *Biorem. J.*, 2008, **12**, 1–11, DOI: **10.1080/10889860701866263**.

35 V. L. Shulman, Tire Recycling, Waste: A Handbook for Management, 2019, 489–515, DOI: **10.1016/B978-0-12-815060-3.00026-8**.

36 L. Moulin, S. Da Silva, A. Bounaceur, M. Herblot and Y. Soudais, Assessment of Recovered Carbon Black Obtained by Waste Tires Steam Water Thermolysis: An Industrial Application, *Waste Biomass Valorization*, 2017, **8**, 2757–2770, DOI: **10.1007/s12649-016-9822-8**.

37 S. Ramarad, M. Khalid, C. T. Ratnam, A. L. Chuah and W. Rashmi, Waste tire rubber in polymer blends: A review on the evolution, properties and future, *Prog. Mater. Sci.*, 2015, **72**, 100–140, DOI: **10.1016/J.PMATSCI.2015.02.004**.

38 A. Quek and R. Balasubramanian, Liquefaction of waste tires by pyrolysis for oil and chemicals—A review, *J. Anal. Appl. Pyrolysis*, 2013, **101**, 1–16, DOI: **10.1016/j.jaap.2013.02.016**.

39 M. Štaffová, F. Ondreáš, J. Svatík, M. Zbončák, J. Jančář and P. Lepcio, 3D printing and post-curing optimization of photo-polymerized structures: Basic concepts and effective tools for improved thermomechanical properties, *Polym. Test.*, 2022, **108**, 107499, DOI: **10.1016/j.polymertesting.2022.107499**.

40 C. Zhou, Y. Wang, X. Huang, Y. Wu and J. Chen, Optimization of ultrasonic-assisted oxidative desulfurization of gasoline and crude oil, *Chem. Eng. Process. Process Intensif.*, 2020, **147**, 107789, DOI: **10.1016/J.CEP.2019.107789**.

41 J. Y. Kim, J. Y. Oh and K. S. Suh, Voltage switchable surface-modified carbon black nanoparticles for dual-particle electrophoretic displays, *Carbon*, 2014, **66**, 361–368, DOI: **10.1016/J.CARBON.2013.09.011**.

42 J. Borrello, P. Nasser, J. C. Iatridis and K. D. Costa, 3D printing a mechanically-tunable acrylate resin on a commercial DLP-SLA printer, *Addit. Manuf.*, 2018, **23**, 374–380, DOI: **10.1016/j.addma.2018.08.019**.

43 M. Dehurtevent, L. Robberecht, J. C. Hornez, A. Thuault, E. Deveaux and P. Béhin, Stereolithography: A new method for processing dental ceramics by additive computer-aided manufacturing, *Dent. Mater.*, 2017, **33**, 477–485, DOI: **10.1016/j.dental.2017.01.018**.